# Near-Range Multipath Mitigation Methodology for Multistatic SAR Applications Using Matched-Adaptive Filters

Filip Rosu [ID], Andrei Anghel [ID], *Senior Member, IEEE*, Silviu Ciochină, *Life Senior Member, IEEE*, Remus Cacoveanu [ID], and Mihai Datcu [ID], *Fellow, IEEE*

*Abstract*—This article presents a methodology based on matched-adaptive filters, which is used to mitigate the effect of near-range multipath in multistatic SAR systems and transponders. It is challenging to physically construct a bistatic receiver such that the reference signal is not leaked into the received signal, either via coupling in the circuitry or via reflections off objects in the vicinity of the receiver. Due to its much larger amplitude, the reference signal can easily mask near-range targets with its sidelobes. A similar signal degradation is observed in active transponders that are used for calibrating radar systems, when objects exist in their vicinity. In this article, we address these two issues: the coupling between the reference channel and the imaging channel, and the parasitic echoes present in the transponder response. A novel methodology is proposed that is capable of time-domain filtering the undesired components in real time. The novelty consists in combining matched and adaptive filters as a means of boosting performance and resolution estimation, resulting in an extremely accurate multipath elimination method. The proposed methodology is experimentally evaluated and optimized for each of the two aforementioned problems.

*Index Terms*—Bistatic and multistatic radar, deconvolution, matched-adaptive filtering, multipath, synthetic aperture radar (SAR).

## I. INTRODUCTION

IN RECENT years, synthetic aperture radar (SAR) instruments have become an essential tool in remote sensing

Filip Rosu and Andrei Anghel are with the Research Centre of Spatial Information, CEOSpaceTech, University POLITEHNICA of Bucharest, 060042 Bucharest, Romania (e-mail: filip.rosu@radio.pub.ro; andrei.anghel@munde.pub.ro).

Silviu Ciochină is with the Telecommunications Department, University POLITEHNICA of Bucharest, 060042 Bucharest, Romania (e-mail: silviu@comm.pub.ro).

Remus Cacoveanu is with the EOS Electronic Systems, 014455 Bucharest, Romania, and also with the Research Centre of Spatial Information, CEOSpaceTech, University POLITEHNICA of Bucharest, 060042 Bucharest, Romania (e-mail: remus.cacoveanu@upb.ro).

Mihai Datcu is with the Remote Sensing Technology Institute, German Aerospace Center, 82234 Weßling, Germany, and also with the Research Centre of Spatial Information, CEOSpaceTech, University POLITEHNICA of Bucharest, 060042 Bucharest, Romania (e-mail: mihai.datcu@dlr.de).

Digital Object Identifier 10.1109/JSTARS.2022.3165470

applications and represent a great interest for space agencies [1]. SAR is capable of providing high-resolution radar images and serves as an extremely useful technique in the field of Earth Observation (EO) [2]. The main advantage of SAR imaging over the conventional optical sensor based imaging is that it can maintain a nominal operation independent of weather changes or sunlight. By using interferometry techniques, displacements can be monitored with an unsurpassed accuracy leading to valuable insight on geological stability [3]–[5].

Apart from displacement measurements, SAR sensors, depending on their operating frequency, offer the possibility of obtaining unique information regarding physical parameters of matter. A couple of such examples are SAR sensors operating in *L* and *P* bands, which are typically used for extracting information on biomass and soil humidity, whereas *C*- or *X*-band sensors are used in applications, such as monitoring ocean currents, oil spills, agriculture, and urban imaging.

A technological advancement of significant value in the field of remote sensing is the multistatic SAR. These spatially distributed and modular systems can improve coverage and adaptability along with enhancing performance and resolution, when compared to the monostatic SAR [6]–[9].

However, realizing such a system poses several challenges, such as meeting highly precise synchronization and timing requirements, and the need of complex calibration methods [10]. Another issue is that bistatic and multistatic radar systems are affected by coupling, either within the circuitry or via reflections from nearby objects, between the reference/synchronization channel and the main receive, or imaging, channel [11]. The reference signal is received from line of sight and has a significantly larger amplitude than the target reflections received by the imaging channel. Because of this, if just a small fraction of the reference signal is coupled to the imaging channel, multiple targets may be masked by the sidelobes of the reference signal's point spread function (PSF). This is one of the two problems addressed in this article, and is illustrated for a spaceborne transmitter (TX)—ground-based receiver (RX) bistatic SAR system in Fig. 1. The problem may be further generalized for fully spaceborne multistatic SAR systems, such as the TanDEM-X [7] or European Space Agency's (ESA) Harmony mission [6].

The second problem addressed in this article is related to the tolerance of spaceborne SAR applications, which is defined by the mission specifications and must be maintained throughout the mission's lifetime [12]. The methods used for calibrating SAR systems typically make use of natural and artificial targets and are of paramount importance for SAR performance
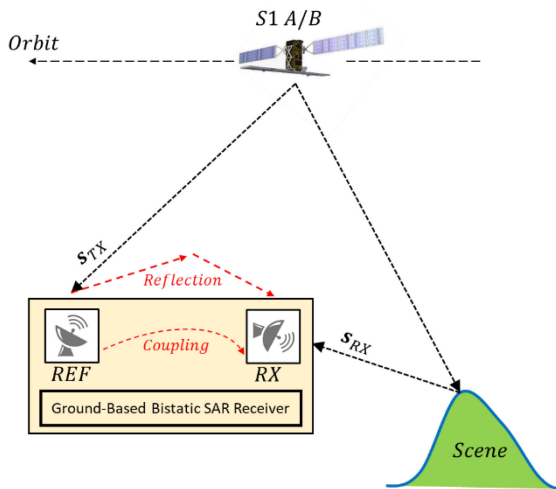
Fig. 1. Spaceborne transmitter—stationary receiver bistatic geometry. The addressed issue is depicted in red, as a parasitic coupling or reflection between the reference channel and the receive channel.



Fig. 2. Calibration transponder used for SAR applications, which is affected by parasitic couplings.

[13], [14]. Natural targets present the most cost-effective calibration method, but they do not always provide a reliable scattering center. Prior work has been done in [12] and [15], where the authors evaluate the performance of natural targets for calibration purposes, and propose a calibration method using multiple passes. For real-time, single-pass calibration, artificial targets, such as corner reflectors or transponders, are often used [16]. Multiple designs of reliable artificial passive targets are provided in [17] and [18]. However, passive targets lack the processing capability and the reduced size that active transponders benefit of, and generally cannot be used in bistatic geometry. Therefore, active transponders, although more expensive and deployable only in limited geographical areas, offer more reliable and dynamic responses than both artificial and natural passive scatterers.

An issue affecting active transponders is the coupling between the TX and RX antennas, which gives rise to undesired multipath and signal degradation. For SAR applications, the antenna spacing is limited so that the transponder behaves as a point target. The relatively small spacing between the TX and RX antennas can easily lead to coupling either directly or through reflection off objects in the vicinity of the transponder. The envisaged geometry is illustrated in Fig. 2. For pulsed radar transponders, a basic approach is to keep the receiver in standby until a certain power level is met, then the data are captured and held in memory for the pulse duration and transmitted afterward, thus eliminating the possibility of any feedback to take place. The drawback of this approach is that a delay comparable to the entire pulse duration, for chirp-based radars, may lead to extreme off-sets in the range profile, making the transponder impractical.

In this article, a methodology is presented, which is capable of solving the two issues mentioned earlier: the leakage of the reference signal in the bistatic SAR image, and the undesired echoes present in transponder responses. The novelty consists in the proposed matched-adaptive filter configuration. The configuration is adapted accordingly to optimize the performance when used to enhance each of the two aforementioned applications.
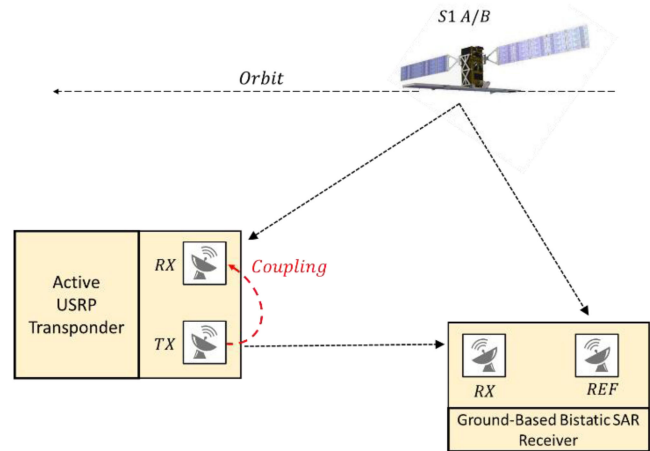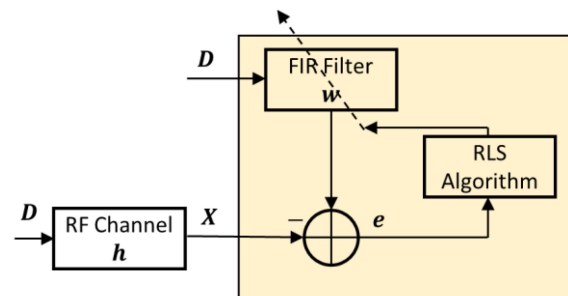


Fig. 3. Traditional channel-estimation configuration for adaptive filters.

The rest of this article is organized as follows: In Section II, a detailed comparison is provided between the traditional adaptive filter and the matched-adaptive filter. In Section III, the first application is presented, including a detailed description of the reference signal coupling problem together with the proposed solution, which is evaluated using experimental data. In Section IV, the second application is presented, where simulated and experimental data are used to evaluate the proposed transponder signal filtering method. Finally, Section V concludes this article.

## II. PROPOSED MATCHED-ADAPTIVE FILTER CONFIGURATIONS

In this section, the proposed matched-adaptive filter methodology is presented. The two main configurations in which an adaptive filter will be placed in are the channel estimation configuration shown in Fig. 3, and the echo-cancellation configuration shown in Fig. 4. In principle, the channel estimation configuration uses an adaptive algorithm to adapt the weights of the finite impulse response (FIR) filter $w$ such that they match the radio frequency (RF) channel $h$. The echo-cancellation configuration adapts the weights until the effect of the RF channel is removed.

In this work, the proposed channel estimation configuration, Fig. 5, is used in the near-range elimination application, while the proposed echo-cancellation configuration, Fig. 6, is used in the second application, to enhance the active transponder response in real-time.

Next, a short description of the recursive least squares (RLS) algorithm will be made, which was the adaptive algorithm used
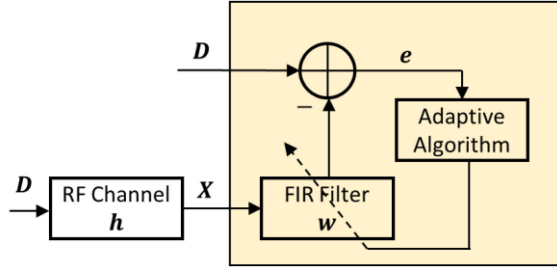
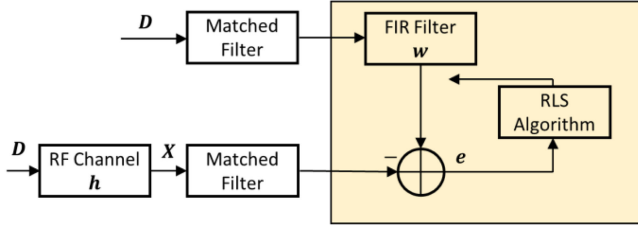Fig. 4. Traditional echo-cancellation configuration for adaptive filters.



Fig. 5. Proposed matched-filtered channel-estimation configuration using the RLS adaptive algorithm.
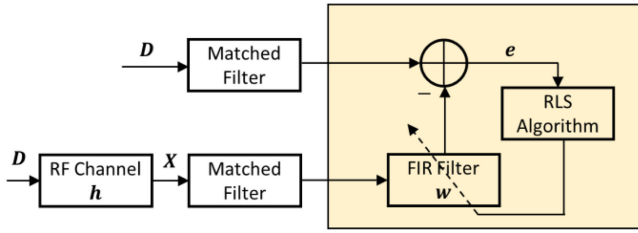


Fig. 6. Proposed matched-filtered echo-cancellation configuration using the RLS adaptive algorithm.

in our research. Unlike other adaptive algorithms, it presents unique capabilities, such as memory and fast convergence, which make it suitable for the proposed matched-adaptive methodology. The least mean squares (LMS) and the normalized LMS (NLMS) adaptive algorithms are widely used in practice for their low complexity, however their convergence rate is slow, requiring multiple samples to be processed [19], [20]. Because of this, signals that are stationary relative to the sampling rate are required, e.g., speech signals. The proposed matched-adaptive methodology is different than what is currently used in practice. The method first makes use of matched filters to compress the signal to only a few samples. It is shown in this work that the RLS is capable of converging to a highly accurate solution even for energy-compressed signals, within a few iterations.

*Side note*: Throughout this article, the index placed in brackets $(n)$ is the iteration # of the RLS algorithm, and the terms in bold represent vectors or matrices, (e.g., $\boldsymbol{x}(n)$ is the time series $\boldsymbol{x}$ when values are measured at iteration $n$ of the RLS algorithm). The subscript is used to denote the sample number (e.g., if $\boldsymbol{y}$ is constructed from the first four samples of $\boldsymbol{x}$, then: $\boldsymbol{y} = \boldsymbol{x}_{1:4}$). The superscript "$H$" represents the Hermitian operator. The symbol "$*$" is the convolution operation and "$\otimes$" is the cross-correlation operation.

**Algorithm 1:** Recursive Least Squares.

---

**Input:** $X$, $D$
**Output:** $w^*$
**Initialize:** $\varepsilon = 1$, $\mathbf{w} = 0$, $P(0) = \varepsilon$
**for** $n = 1, \dots$ **do**
$\quad x(n) = \mathbf{X_{n:n+N}}$
$\quad \mathrm{d}(n) = \mathbf{D_n}$
$\quad z(n) = \boldsymbol{x}^H(\boldsymbol{n})\boldsymbol{P}(\boldsymbol{n}-1)$
$\quad \boldsymbol{k}(n) = \frac{z^H(n)}{\lambda + z(n)x(n)}$
$\quad \alpha(\mathrm{n}) = \boldsymbol{d}(\boldsymbol{n}) - \boldsymbol{w}^H(\boldsymbol{n}-1)\boldsymbol{x}(\boldsymbol{n})$
$\quad \boldsymbol{w}(\boldsymbol{n}) = \boldsymbol{w}(\boldsymbol{n}-1) + \boldsymbol{k}(\boldsymbol{n})\boldsymbol{\alpha}^*(\boldsymbol{n})$
$\quad \mathrm{P}(\boldsymbol{n}) = \frac{1}{\lambda}(\boldsymbol{P}(\boldsymbol{n}-1) - \boldsymbol{k}(\boldsymbol{n})\boldsymbol{z}(\boldsymbol{n}))$
**end for**

---

The goal of the RLS algorithm is to minimize the cost function in (1)

$$J(n) = \sum_{i=1}^{n} \lambda^{n-i} |e(i)|^2 \qquad (1)$$

where $e(i)$ is the a posteriori error (2)

$$e(n) = d(n) - \boldsymbol{w}^H(n)\boldsymbol{x}(n) \qquad (2)$$

and $\lambda$ is the forgetting factor, which plays the role of increasing the weight of newer samples over older ones, $d(n)$ is the desired or reference signal, and $\boldsymbol{w}^H(n)\boldsymbol{x}(n)$ is the inner product of the input signal $\boldsymbol{x}(n)$ and the filter coefficients $\boldsymbol{w}^H(n)$ at iteration $n$.

The cost function is minimized when (3) is satisfied

$$\boldsymbol{w}(n) = \boldsymbol{\psi}^{-1}(n)\boldsymbol{\theta}(n) \qquad (3)$$

where $\boldsymbol{\psi}(n)$ is the weighted auto-covariance matrix

$$\boldsymbol{\psi}(n) = \sum_{i=1}^{n} \lambda^{n-i}\boldsymbol{x}(i)\boldsymbol{x}^H(i) \qquad (4)$$

and $\boldsymbol{\theta}(n)$ is the weighted cross-covariance vector

$$\boldsymbol{\theta}(n) = \sum_{i=1}^{n} \lambda^{n-i}\boldsymbol{x}(i)d^*(n). \qquad (5)$$

The recursive relation between $\boldsymbol{w}(n)$ and $\boldsymbol{w}(n-1)$ is based on the recursive properties of $\boldsymbol{\psi}(n)$ and $\boldsymbol{\theta}(n)$

$$\boldsymbol{\psi}(n) = \lambda\boldsymbol{\psi}(n-1) + \boldsymbol{x}(n)\boldsymbol{x}^H(n) \qquad (6)$$

$$\boldsymbol{\theta}(n) = \lambda\boldsymbol{\theta}(n-1) + \boldsymbol{x}(n)d^*(n). \qquad (7)$$

Such that

$$\boldsymbol{w}(n) = \boldsymbol{w}(n-1) + \boldsymbol{k}(n)\alpha^*(n). \qquad (8)$$

A typical implementation of the RLS adaptive filter is shown in Algorithm 1. A more performant adaptation can be found in [21]. The input signals to the RLS algorithm are $\boldsymbol{x}$ and $d$, which represent the received signal and the reference signal, the order depending on the used configuration. $\boldsymbol{\psi}^{-1}(n)$ has been denoted as $P(\mathrm{n})$, $\alpha(n)$ represents the innovation vector, and $\boldsymbol{k}(n) = \boldsymbol{P}(n)\boldsymbol{x}(n)$ represents the Kalman gain.

The RLS complexity per iteration is given by $O(N^2)$ additions and $O(N^2)$ multiplications, where $N$ is the total number of filter taps. The number of iterations depends on the total number of
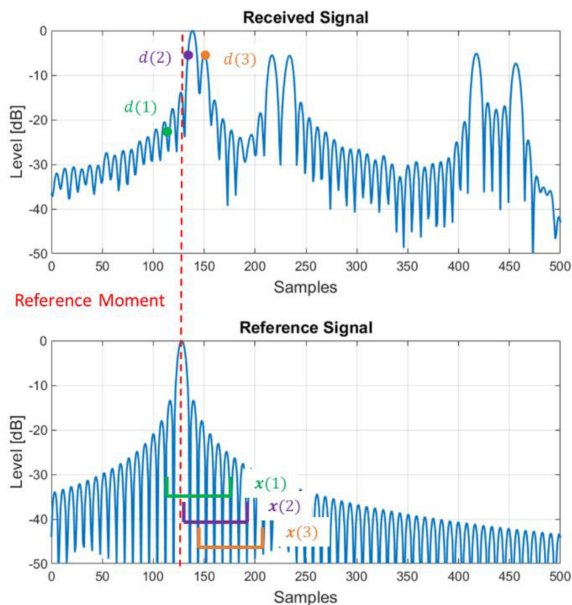
Fig. 7. Example of how data are sequentially processed using a sliding window for the proposed matched-adaptive filter methodology. The reference moment is characterized by $w_1(n)$. The length of $x(n)$ is $N$, and is equal to the order of the FIR filter $w(n)$.

available samples provided by the signals $X$ and $D$. The signals $x(n)$ and $d(n)$ are constructed using a sliding window of size $N$ from the signals $X$ and $D$, where $N$ is the order of the filter $w^H$.

The novelty of the proposed method consists in the introduction of the matched filter reducing the total size of the input signal to just a few samples. This results in significantly less iterations of the adaptive algorithm, but requires faster convergence. This is achieved by replacing the traditional LMS/NLMS algorithms with the more advanced RLS algorithm that is otherwise rarely used in practice due to its high complexity. However, when used in the proposed methodology, it is both faster and more performant than traditional approaches. Although the RLS algorithm requires more operations per iteration than the LMS or NLMS, by using the matched filter, the number of iterations is greatly reduced. As an example, consider that the number of iterations is proportional to the samples available in $X$, which for typical time-domain signals can be 1000, but after matched filtering, $X$ is reduced up to 10 samples, thus reducing the amount of iterations by a factor of 100.

A detailed illustration is shown in Fig. 7 of how the two input signals $x(n)$ and $d(n)$ are selected from the available data $X$ and $D$ using a sliding window. The available data $X$ and $D$ represent the output of a matched filter in a radar use-case, such that the upper plot is in fact a range profile. The size of $x(n)$ and $d(n)$ is equal to the size of the sliding window, which is given by the length of the FIR filter $w$. It is clear that for such energy compressed signals after a few iterations, the reference signal's properties will change drastically, resulting in a very poor performance of the adaptive algorithm. For this reason, we have chosen to use the RLS adaptive algorithm, which is capable of memorizing the effect of the samples in previous windows.

The reference moment expressed as a dashed vertical line through the center of the reference PSF marks the beginning of the acquisition.

## III. APPLICATION I, TX–RX COUPLING REMOVAL IN BISTATIC SAR

### A. Description

This section addresses the issue of TX–RX coupling in bistatic receivers, as previously illustrated in Fig. 1. The passive receiver uses a line-of-sight reference channel, REF, for data synchronization, and a separate receive channel, RX, for capturing the signal reflected from the scene. The measured bistatic time delay for a given target is relative to the moment of arrival of the pulse at the reference channel. Additional space-time synchronization is also required, and for the system presented in this article, this can be achieved using the public ancillary data from ESA, as detailed in previous work [22]. The captured reference signal is used to construct the matched filter for range compression.

In bistatic SAR applications that use multiaperture focusing [9], the coupling will change during the acquisition, hence an adaptive method should be used. A naive approach is to zero the peaks in the range-compressed signal. This solution reduces the dynamic range of the SAR image, but does not deal with the remaining sidelobe.

In contrast to prior art, such as Sornmo *et al.* [23], our method is not limited by the constraint of having nonoverlapping pulses, thus being able to resolve subresolution targets. The authors in [24] present a method in which the matched filter is placed within the adaptive filter loop, and was designed for electrocardiography measurements. However, if the order of the filter is large, an exhaustive amount of computations would be required and will deny real-time capabilities.

### B. Proposed Solution

The reference signal $s_{\mathrm{TX}}$ is received by the reference channel directly from the transmitter, $s_{\mathrm{RX}}$ is the captured raw data, $h_c$ is the radio channel response that contains information regarding target location, amplitude, and phase shift, and $z$ is the receiver noise. The proposed method makes use of a matched-adaptive filter that is placed in channel estimation configuration, as shown in Fig. 8(a). After estimating the channel transfer function, the time-domain received signal can be easily filtered, eliminating the parasitic reference signal from the image, as shown in Fig. 8(b).

At the receiver, the signal can be expressed as the convolution between the reference signal $s_{\mathrm{TX}}$ and the channel response $h_c$

$$s_{\mathrm{RX}} = s_{\mathrm{TX}} * h_c + z. \tag{9}$$

Next, $r_{\mathrm{RX}}$ is the result of matched-filtering $s_{\mathrm{RX}}$, such that

$$r_{\mathrm{RX}} = s_{\mathrm{TX}} \otimes s_{\mathrm{RX}}. \tag{10}$$

In order to identify $h_c$, an adaptive filter is used where $r_{\mathrm{RX}}$ represents the "input signal" and the "desired signal" is

$$r_{\mathrm{TX}} = s_{\mathrm{TX}} \otimes s_{\mathrm{TX}}. \tag{11}$$

Traditional approaches [25], [26] use $s_{\mathrm{RX}}$ and $s_{\mathrm{TX}}$ as inputs to the adaptive filter, but this requires all fast-time samples to be processed, which is computationally exhaustive. The proposed method only requires a few samples to be analyzed, as most signal information regarding targets/multipath is embedded in just a few samples after matched filtering is applied. The convergence rate is improved by the proposed method due to the much higher signal-to-noise ratio (SNR). Once convergence state has been reached, the adaptive filter will have an impulse response
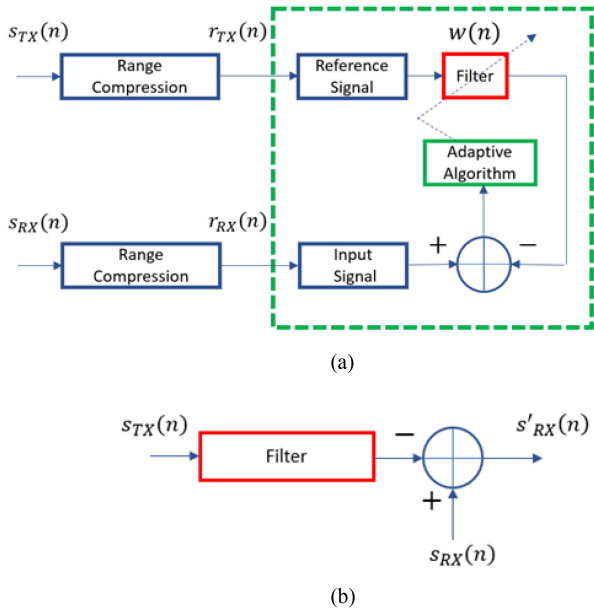
Fig. 8.    Block representation (a) of the proposed channel estimation scheme for estimating the weight vector $w(n)$, and (b) of the proposed method used to eliminate the reference signal components from the received signal.



Fig. 9.    (a) Reference signal $s_{\mathrm{TX}}$. (b) Received signal during a single pulse acquisition represented in fast-time $s_{\mathrm{RX}}$. (c) First 500 m of the range-compressed reference signal $r_{\mathrm{TX}}$. (d) First 500 m of the range-compressed received signal $r_{\mathrm{RX}}$.

function $w$ equal to the first $N$ samples of the discretized radio channel response $h_c$.

The final step is to subtract $s_{\mathrm{TX}} * w$ from the raw data's respective isoazimuth line

$$s'_{\mathrm{RX}} = s_{\mathrm{RX}} - s_{\mathrm{TX}} * w. \qquad (12)$$

The number of eliminated signal components $N$ is equal to the adaptive filter's order, hence to eliminate a larger area, an adaptive filter with more filter taps is required. The adaptive filter $w$ replaces the PSF with a single sample, the proposed method can correctly eliminate targets spaced closer than the range resolution. More importantly, the spillover and sidelobes of the targets within the first $N$ samples are eliminated from the entire signal. The method processes each PRI separately; therefore, the Doppler effect is negligible, even more so for the presented bistatic SAR acquisition system.

### C. Experimental Results

In this section, we will present the performance of the proposed method applied on data acquired from a spaceborne transmitter—ground-based receiver bistatic SAR system [22]. The opportunistic satellite is Sentinel 1-A operating in interferometric wide swath mode, and the ground-based receiver is placed on the roof-top of one of the highest buildings in Bucharest, Romania—the Faculty of Electronics and Telecommunications, UPB. The purpose of this experiment is to eliminate all reflections within $R_e = 10$ m, equivalent to eliminating all signal components captured by the receiver within 67 ns since the reference signal has been received. $R_e$ should be chosen as the longest undesired physical path between the REF channel and the RX channel. The reference signal used for range compression during a single pulse acquisition is shown in Fig. 9(a). The fast-time signal received during the pulse acquisition is shown
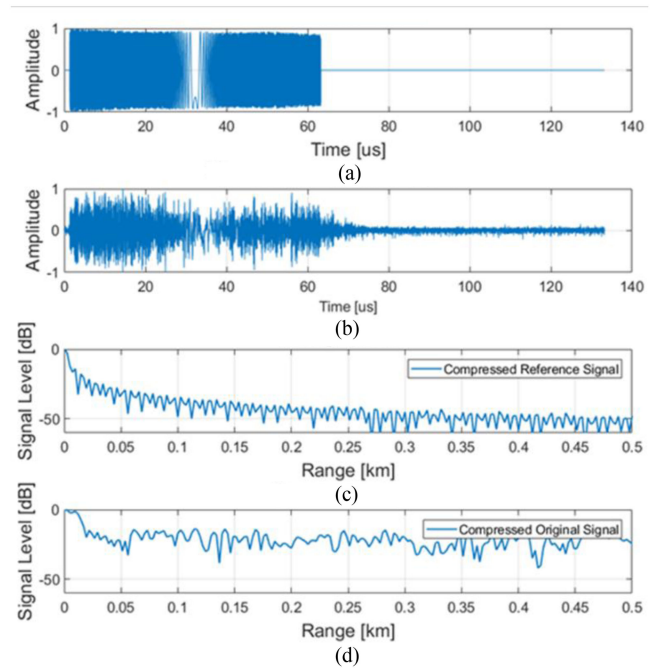
in Fig. 9(b). The range-compressed reference and original signals are shown in Fig. 9(c) and (d), respectively. The parasitic coupling is formed as multiple reflections between 2.5 and 9.5 m from the receiver.

Traditional methods use $s_{\mathrm{TX}}$ and $s_{\mathrm{RX}}$, depicted in Fig. 9(a) and (b), respectively, as a means of estimating the channel transfer function, as opposed to the proposed method that uses $r_{\mathrm{TX}}$ and $r_{\mathrm{RX}}$, depicted in Fig. 9(c) and (d), respectively. We will further compare the performance of the proposed method with an adaptive filter method and with the naive deconvolution via frequency division method.

The order of the adaptive filter was chosen as: $N = F_s \frac{2R_e}{c}$, where $R_e = 10$ m is the elimination range, $F_s$ is the analog digital converter sampling frequency, and $c$ is the speed of light. In this experiment, the sampling frequency is $F_s = 60$ MHz, resulting in an adaptive filter size of 4. The performance of the proposed method can be visually evaluated from the range-compressed SAR data shown in Fig. 10. The evolution of the adaptive filter coefficients when placed in the proposed configuration is presented in Fig. 11. Next, an arbitrary isorange profile from Fig. 10 is analyzed in detail. It is shown that the traditional adaptive-filter approach [see Fig. 12(c)] is less effective in eliminating the reference signal components than the proposed method, as shown in Fig. 12(e).

The proposed method eliminates the coupled signal precisely, revealing multiple targets initially masked by sidelobes, which can be visible up to 50 m. The proposed method is also computationally faster, as the matched-adaptive filter's inputs, $r_{\mathrm{RX}}$ and $r_{\mathrm{TX}}$, only require a few samples, 16 in this example, whereas the traditional adaptive filter's inputs, $s_{\mathrm{RX}}$ and $s_{\mathrm{TX}}$, are spread over 8000 samples. The RLS complexity, as presented in Algorithm 1, is $5N^2 + N$ per iteration, where $N$ is the filter size. The number of iterations is given by the input signal's length. Since both
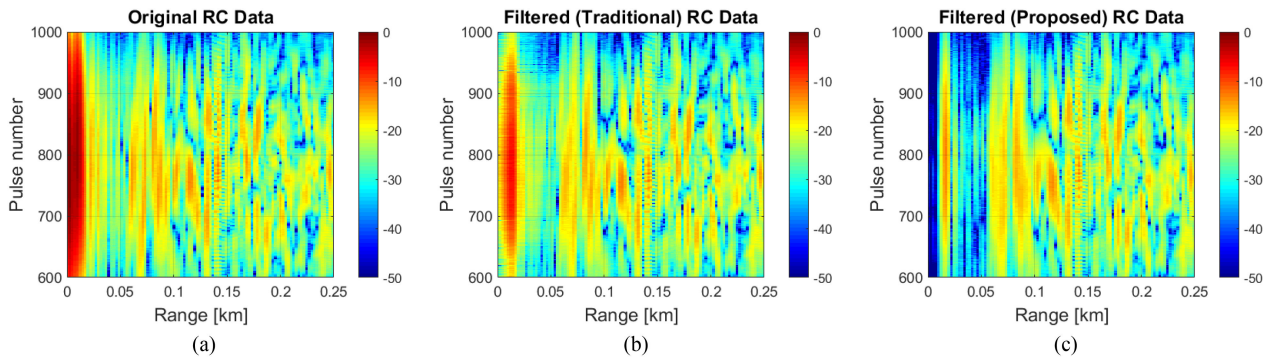
Fig. 10. Range-compressed SAR image (a) of the raw data, (b) of the near-range filtered targets using traditional approach, and (c) of the near-range filtered targets using proposed approach.
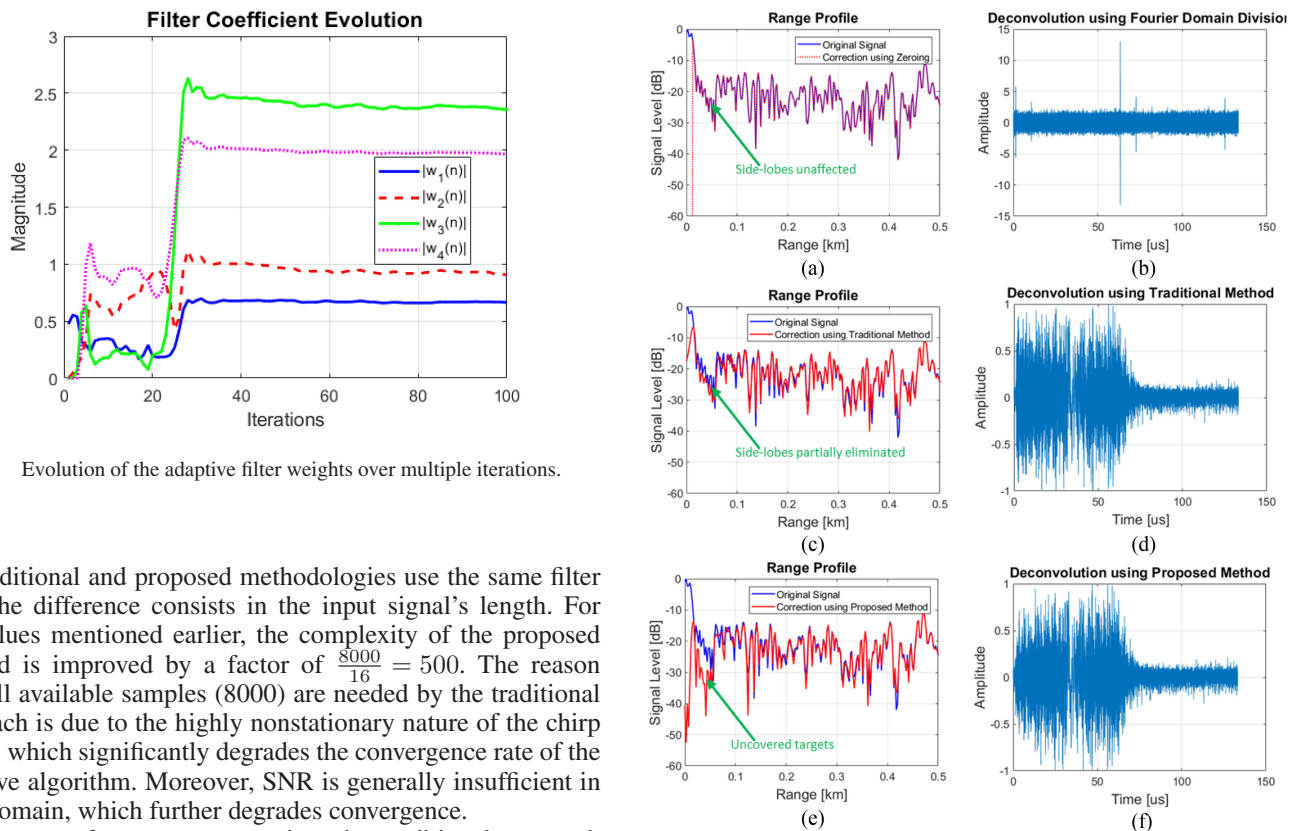


Fig. 11. Evolution of the adaptive filter weights over multiple iterations.



Fig. 12. Range profile from which targets within 10 m of the receiver have been eliminated: (a) with proposed method using a matched-adaptive filter, (c) with the traditional approach using an adaptive filter, (e) by zeroing the first samples. The original range profile is in blue, and the processed range profiles are drawn in red. Fast-time signal reconstruction using (b) the proposed method, (d) the traditional adaptive filter method, and (f) zeroing in the range-profile and applying deconvolution.

the traditional and proposed methodologies use the same filter size, the difference consists in the input signal's length. For the values mentioned earlier, the complexity of the proposed method is improved by a factor of $\frac{8000}{16} = 500$. The reason why all available samples (8000) are needed by the traditional approach is due to the highly nonstationary nature of the chirp signal, which significantly degrades the convergence rate of the adaptive algorithm. Moreover, SNR is generally insufficient in time domain, which further degrades convergence.

From a performance perspective, the traditional approach using adaptive filters eliminates the multipath only partially, and does not deal with the sidelobes as effectively. Performance could be slightly improved for the traditional approach, by increasing the filter size, $N$, by a factor determined empirically, however, this would lead to an even higher computational cost. Finally, the naive method presented in Fig. 12(a) consists in zeroing the first $N$ cells of the range profile, and applying deconvolution via frequency-domain division. It is evident that this has no effect on the sidelobes of the eliminated targets, which continue to exist. Moreover, the raw data are difficult to be recovered by deconvolution, as shown in Fig. 12(b). This is due to the deconvolution problem described previously in [11]. The signals presented in Fig. 12(f) and (d) represent the fast-time signals without the signal returns that originated within a 10-m range, filtered by the proposed method and the traditional adaptive filter method, respectively. The near-range results from Fig. 12 are presented in greater detail in Fig. 13.

## IV. APPLICATION II, ENHANCING THE CALIBRATION TRANSPONDER RESPONSE

### A. Description

The present application is based on the radar transponder described in previous work [27], which is compatible with Sentinel 1-A/B satellites and used for ground-based receiver bistatic or multistatic applications. The transponder provides an artificial method of increasing signal-to-clutter ratio by digitally
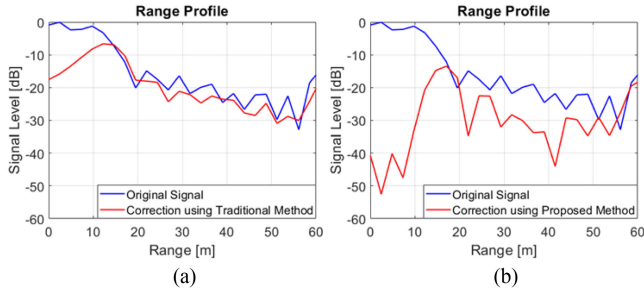
Fig. 13. Range profiles (a) from Fig. 12(c), and (b) from Fig. 12(e), represented between 0 and 60 m.
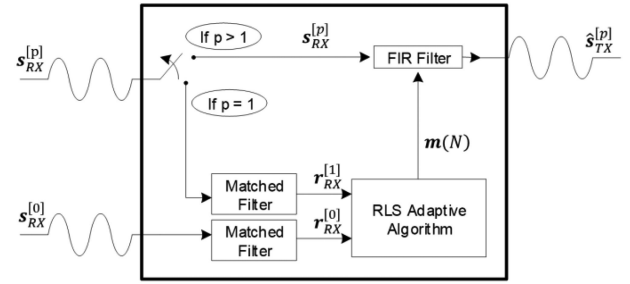


Fig. 14. Simplified block schematic of the proposed real-time method. $s_{RX}^{[p]}$ is the input of the transponder and $s_{TX}^{[p]}$ is the output.

adding a path delay to the received pulse, which allows a good separation in the range profile between the re-emitted signal and the clutter generated by the natural reflections off the transponder (and the building it is placed on). Even without any clutter, the original response of the transponder was not ideal and presented artefacts [28]. These were caused by the feedback between the TX and RX due to coupling between the antennas or reflections off objects in the vicinity of the active transponder

$$s_{TX} = s_{RX} * g \tag{13a}$$

where $s_{RX}$ and $s_{TX}$ are the signals received and transmitted by the transponder, respectively, and $g$ is the multipath weight function. It is desired to have $s_{TX} = s_{RX}$, where for simplicity, we ignore the amplitude gain and phase shift caused by the transponder. Furthermore, we will rename the weight function of the echo-canceller adaptive filter as $m(n)$ to clearly distinguish it from the channel estimation filter $w(n)$ introduced in the previous section. Equation 10(a) can be written in frequency domain as

$$S_{TX} = S_{RX} G \tag{13b}$$

where $S_{RX}$, $S_{TX}$, and $G$ are the Fourier transforms of $s_{RX}$, $s_{TX}$, and $g$, respectively. In steady state, we are dealing with a feedback situation rather than traditional multipath, resulting in $g$ to have an autoregressive model, equivalent to $G$ being a pole-only transfer function.

Because of this, the proposed solution is to use a similar approach as in the previous section. The difference is that instead of using a channel-estimation configuration, an echo-cancellation configuration will be used instead.

Before presenting the proposed solution, it will be shown that traditional adaptive filter methodologies cannot provide a valid solution for this problem.

The echo-cancellation configuration implies that the two inputs of the adaptive algorithm are now switched, $s_{TX}$ is the input signal of the RLS adaptive algorithm, and $s_{RX}^{[0]}$ represents the desired signal. $s_{RX}^{[0]}$ is the ideal version of the received signal, $s_{RX}$, when the transponder's transmitter is turned OFF. The superscript "[p]" denotes the pulse number from the SAR image, which starts from "[1]," with exception of the reference pulse, which has superscript "[0]." In order to obtain $s_{RX}^{[0]}$, the transponder captures a pulse while keeping the TX OFF, such that there is no feedback or multipath during receive. After $s_{RX}^{[0]}$ has been captured, it is used to correct/process all future acquisitions $s_{RX}^{[p]}$.

The cost function of the echo-cancellation RLS adaptive algorithm is minimized when

$$M = G^{-1} \tag{14}$$

such that the adaptive filter's output after $n$ iterations is

$$\hat{s}_{TX} = s_{TX} * m(n) \tag{15a}$$

$$\hat{S}_{TX} = S_{RX} M(n) \tag{15b}$$

where $\hat{s}_{TX}$ is the output of the adaptive filter, $\hat{S}_{TX}$ and $M$ are the Fourier transforms of $\hat{s}_{TX}$ and $m$, respectively. In this application, $G$ is stable transfer pole-only function, meaning that $M$ is a minimum phase transfer function, and therefore it can be implemented as a stable FIR filter.

A major issue is that unlike in the channel-estimation method, the echo-cancelling output $\hat{s}_{TX}$ does not preserve phase information

$$\hat{s}_{TX}^{[p]} = s_{RX}^{[p]} * g * m(n). \tag{16}$$

After the last iteration of the adaptive filter, ideally the transponder will transmit

$$\hat{s}_{TX}^{[p]} = s_{RX}^{[0]} \tag{17}$$

where $\hat{s}_{TX}^{[p]}$ is the filtered signal that is going to be transmitted by the transponder instead of $s_{TX}^{[p]}$. Equation (17) shows that each pulse will have its phase set to that of the reference signal. This phase derotation will make SAR imaging impossible.

*B. Proposed Solution*

The novel implementation that is proposed in this article solves the phase derotation issue while also significantly reducing computational cost. It requires that only the first radar pulse $s_{RX}^{[1]}$ is processed by a matched-adaptive filter

$$r_{RX}^{[1]} = s_{RX}^{[1]} \otimes s_{RX}^{[0]}. \tag{18}$$

The reference pulse matched filtering can be precomputed and saved in memory

$$r_{RX}^{[0]} = s_{RX}^{[0]} \otimes s_{RX}^{[0]}. \tag{19}$$

The two inputs of the adaptive algorithm are: the matched filter output of the first pulse $r_{RX}^{[1]}$ and the ideal auto-correlation $r_{RX}^{[0]}$, as shown in Fig. 14. The signals must first be circular shifted accordingly, at least by $N$ samples, such that they resemble Fig. 7.
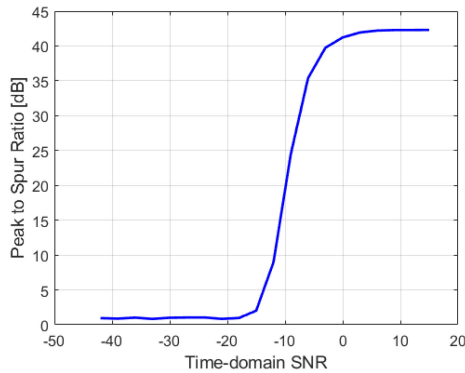
Fig. 15. Peak-to-spur ratio versus SNR.



Fig. 16. Ideal, nonprocessed, and processed range-compressed signals, for an input signal of 15-dB SNR containing additional subresolution multipath propagation, observable in the nonprocessed signal.

This is required in order to preserve the symmetry of the reference pulse. The outputs of the adaptive algorithm are the weights of the FIR filter $\boldsymbol{m}(n)$. After $2N$ iterations, the $N$ coefficients of the adaptive filter are implemented as a traditional FIR filter, and used to filter the real-time time-domain acquisition, which is amplified and retransmitted

$$\hat{\boldsymbol{s}}_{\mathrm{TX}}^{[p]} = \left( \boldsymbol{s}_{\mathrm{RX}}^{[p]} * \boldsymbol{g} \right) * \boldsymbol{m} \qquad (20)$$

As previously mentioned, for simplicity, we ignore the amplitude gain of the transponder.

The FIR filter will suppress the parasitic couplings and will introduce the same phase derotation to all radar pulses, hence the relative phase information between adjacent pulses is perfectly preserved. The method only uses a small number of iterations, which is proportional to the FIR filter order. The method also eliminates the need of using a matched filter for every pulse, which will significantly affect real-time capabilities given the large size of the signal in time domain. Because the coupling generally appears as a series of closely spaced peaks, only the first few coefficients from the range profile are necessary to model the coupling, thus the size of the static FIR filter will be orders of magnitude smaller than the matched filter.

### C. Simulated Results

Along with all the benefits presented up to this point, the matched filtering also increases the signal's SNR. The SNR of the range compressed signal, which is fed to the adaptive algorithm, is increased by $10\log(Ns)$, where $Ns$ represents the number of in-phase/quadrature samples in which the matched filtering has been done. For the present application, a typical value of $Ns$ is 6000, resulting in a 38-dB SNR increase. Fig. 15 presents a measure of performance of the proposed method as a function of SNR. It is computed as the ratio between the largest peak of the compressed signal and second largest peak, which at high SNR is the main-lobe to sidelobe ratio of the PSF, and at low SNR is given by spurs, noise, and unresolved targets.

The performance of the proposed method for –15-dB and +15-dB SNR is presented in Figs. 16 and 17. The received signal is composed from the direct signal and a subresolution multipath, resulting in a widened PSF. It can be seen that if the SNR is large enough, the proposed method easily deals with the subresolution multipath, and also acts as a denoising filter.
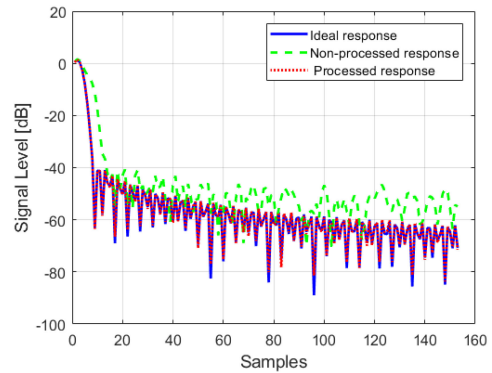


Fig. 17. Ideal, nonprocessed, and processed range-compressed signals, for an input signal of –15-dB SNR containing additional subresolution multipath propagation, observable in the nonprocessed signal.
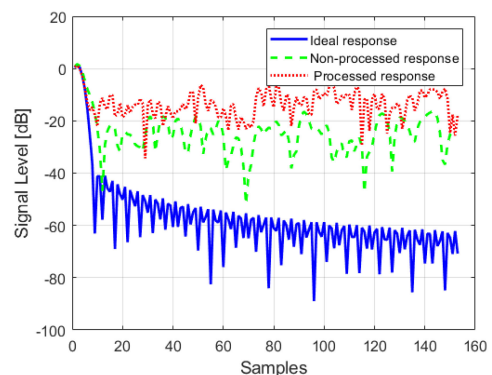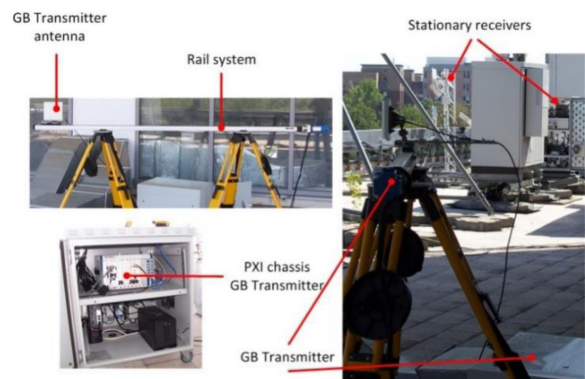


Fig. 18. Ground based bistatic SAR system placed on the rectorate building of UPB.

### D. Experimental Results

The experimental setup is shown in Figs. 18 and 19. The ground-based bistatic SAR system is presented in Fig. 18, whereas the distributed system is shown in Fig. 19. The receiver and transmitter, as shown in Fig. 18, are approximately 10-m apart, placed on top of the rectorate building of the Polytechnic University of Bucharest. The transponder is placed at 700 m in one of the highest points in Bucharest city, the main building of the Faculty of Electronics and Telecommunications (ETTI).

Fig. 19.    Transceiver, transponder, and illuminated scene as seen from Google maps.
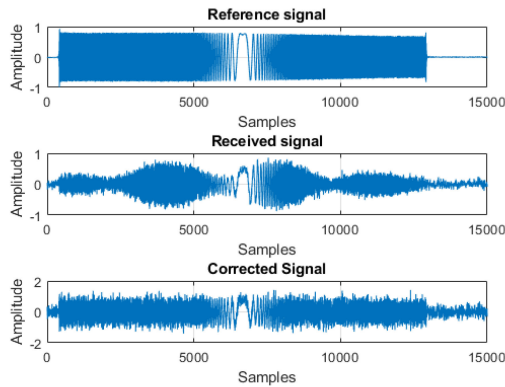


Fig. 20.    Time-domain representation of the reference, received, and corrected signals.
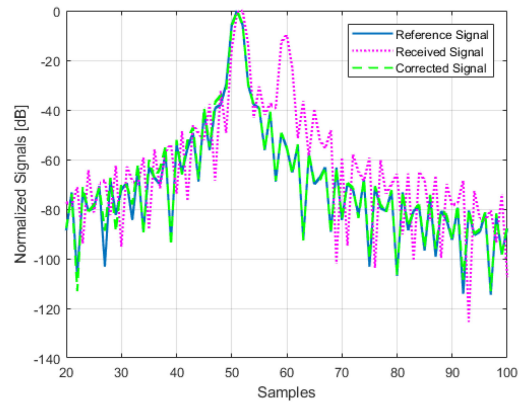


Fig. 21.    Range compression of the reference, received, and corrected signals, represented in continuous blue, dotted magenta, and dashed green lines, respectively.
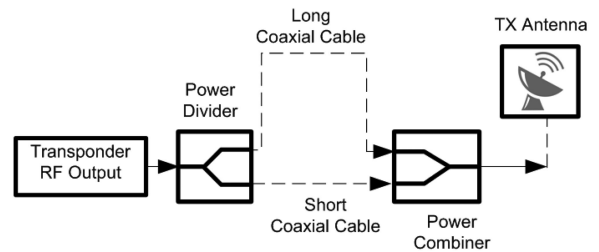


Fig. 22.    Block schematic presenting additional multipath artificially introduced by transponder.
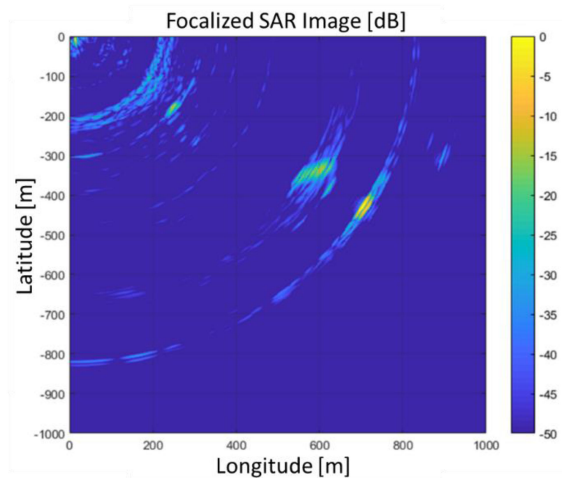


Fig. 23.    SAR image of the scene depicted in Fig. 18.

Our central frequency is 5.755 GHz with a bandwidth of 48 MHz and pulse duration of 50 $\mu$s. The central frequency was chosen close to that of the Sentinel-1A/B, 5.405 GHz, so that the same transponder hardware could be used for either ground-based or spaceborne bistatic SAR applications.

Acquired data are first processed using MATLAB. The data consist in range profiles saved from a SAR acquisition of the scene shown in Fig. 19. The time-domain waveforms of the reference, received, and corrected signals are presented in Fig. 20. The respective range profiles are presented in Fig. 21. The second peak corresponds to an artificial delay that was generated using the system in Fig. 22. Aside from the hardware generated peak, another subresolution echo was digitally added by adding a slightly shifted copy of the signal to itself. This was done to create a very large undesired component both at subresolution range and at a larger distance. This experiment shows that the method is capable of subresolution multipath mitigation.

The subresolution echo can be observed from the larger width of the main lobe. The correction solves undesired multipath and correctly filters the desired signal, even when subresolution echoes are present. It has been considered that the radio channel of the multipath is stationary for long enough for the processing to be done correctly, allowing us to use the echo-cancelling configuration of the proposed method, which consists in implementing the FIR filter previously computed in MATLAB. Fig. 23 displays the image of the illuminated scene from Fig. 19, where the RX and TX are placed at (0, 0) and the transponder is placed at near (−350, 600) where its natural reflection can be observed and its active response is observed at (−450, 700). Fig. 24 compares the transponder response with and without correction.

The level difference between the transmitted signal and the artificial multipath interference, as shown in Fig. 24, is 10 dB larger with the proposed method. The FIR filter coefficients were
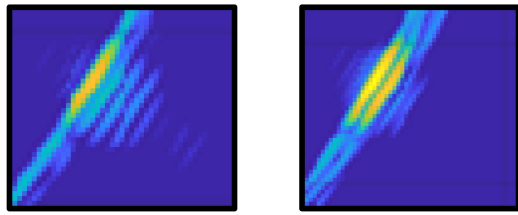
Fig. 24. Transponder response with and without the implemented echo-cancelling filter.

computed using an acquisition one week prior to the day the presented data were captured.

## V. CONCLUSION

A near-range target signature elimination methodology has been presented. The method uses highly compressed signals as an input to the memory preserving RLS adaptive algorithm as a means of quickly converging to the desired solution. Two different applications are presented, a bistatic SAR receiver affected by near-range reflections, and an active transponder affected by TX–RX coupling and multipath. Numerical simulations are presented as a means of providing a clear understanding of the limitations and capabilities of the proposed methodology. Experimental results are presented for both use cases and outline how the two aforementioned applications perform with and without the proposed methodology. Future work will consist in implementing both methods using LabView for real-time operation and analyzing the possibility of using the proposed method to enhance fully spaceborne multistatic SAR systems.

## REFERENCES

[1] A. Moreira, "A golden age for spaceborne SAR systems," in *Proc. 20th Int. Conf. Microw. Radar Wireless Commun.*, 2014, pp. 1–4.

[2] A. Moreira, P. Prats-Iraola, M. Younis, G. Krieger, I. Hajnsek, and K. P. Papathanassiou, "A tutorial on synthetic aperture radar," in *IEEE Geosci. Remote Sens. Mag.*, vol. 1, no. 1, pp. 6–43, Mar. 2013.

[3] O. Monserrat, M. Crosetto, and G. Luzi, "A review of ground-based SAR interferometry for deformation measurement," *ISPRS J. Photogramm. Remote Sens.*, vol. 93, pp. 40–48, 2014.

[4] R. Iglesias *et al.*, "Ground-based polarimetric SAR interferometry for the monitoring of terrain displacement phenomena–Part II: Applications," *IEEE J. Sel. Topics Appl. Earth Observ. Remote Sens.*, vol. 8, no. 3, pp. 994–1007, Mar. 2015.

[5] R. Iglesias *et al.*, "Ground-based polarimetric SAR interferometry for the monitoring of terrain displacement phenomena–Part I: Theoretical description," *IEEE J. Sel. Topics Appl. Earth Observ. Remote Sens.*, vol. 8, no. 3, pp. 980–993, Mar. 2015.

[6] P. López-Dekker, H. Rott, P. Prats-Iraola, B. Chapron, K. Scipal, and E. D. Witte, "Harmony: An earth explorer 10 mission candidate to observe land, ice, and ocean surface dynamics," in *Proc. IEEE Int. Geosci. Remote Sens. Symp.*, 2019, pp. 8381–8384.

[7] M. Zink *et al.*, "TanDEM-X: 10 years of formation flying bistatic SAR interferometry," *IEEE J. Sel. Topics Appl. Earth Observ. Remote Sens.*, vol. 14, pp. 3546–3565, Feb. 2021.

[8] S. Leinss and P. Bernhard, "TanDEM-X: Deriving InSAR height changes and velocity dynamics of Great Aletsch glacier," *IEEE J. Sel. Topics Appl. Earth Observ. Remote Sens.*, vol. 14, pp. 4798–4815, May 2021.

[9] F. Rosu, A. Anghel, R. Cacoveanu, B. Rommen, and M. Datcu, "Multiaperture focusing for spaceborne transmitter/ground-based receiver bistatic SAR," *IEEE J. Sel. Topics Appl. Earth Observ. Remote Sens.*, vol. 13, pp. 5823–5832, Sep. 2020.

[10] B. Brautigam, J. H. Gonzalez, M. Schwerdt, and M. Bachmann, "TerraSAR-X instrument calibration results and extension for TanDEM-X," *IEEE Trans. Geosci. Remote Sens.*, vol. 48, no. 2, pp. 702–715, Feb. 2010.

[11] F. Rosu, A. Anghel, R. Cacoveanu, S. Ciochină, and M. Datcu, "Deconvolution method for eliminating reference signal coupling/reflections in bistatic SAR," in *Proc. IEEE Int. Geosci. Remote Sens. Symp. IGARSS*, 2021, pp. 2715–2718.

[12] P. Guccione, M. Scagliola, and D. Giudici, "Low-frequency SAR radiometric calibration and antenna pattern estimation by using stable point targets," *IEEE Trans. Geosci. Remote Sens.*, vol. 56, no. 2, pp. 635–646, Feb. 2018.

[13] W. M. Kemp and N. M. Martin, "A synthetic aperture radar calibration transponder at C-band," in *Proc. IEEE Int. Conf. Radar*, Arlington, VA, USA, 1990, pp. 81–85.

[14] K. Dumper, C. H. Buck, and A. W. J. Dawkins, "Cost-effective calibration transponders for future synthetic aperture radars," in *Proc. Int. Geosci. Remote Sens. Symp.*, Hamburg, Germany, 1999, pp. 416–418.

[15] D. D'Aria, A. Ferretti, A. M. Guarnieri, and S. Tebaldini, "SAR calibration aided by permanent scatterers," *IEEE Trans. Geosci. Remote Sens.*, vol. 48, no. 4, pp. 2076–2086, Apr. 2010.

[16] K. Dumper, C. Buck, S. R. Day, D. King, and P. E. Gomm, "Design and performance of the prototype advanced SAR calibration transponder," in *CEOS SAR Workshop*, Ulm, Germany, 2004.

[17] Y. Zhou, C. Li, L. Tang, C. Gao, L. Ren, and L. Ma, "Permanent target for synthetic aperture radar image resolution assessment," in *Proc. IEEE Int. Geosci. Remote Sens. Symp.*, 2015, pp. 4284–4287.

[18] C. M. Schmid, R. Feger, and A. Stelzer, "Millimeter-wave phase-modulated backscatter transponder for FMCW radar applications," in *Proc. IEEE MTT-S Int. Microw. Symp.*, 2011, pp. 1–4.

[19] C. Paleologu, S. Ciochina, and J. Benesty, "Variable step-size NLMS algorithm for under-modeling acoustic echo cancellation," *IEEE Signal Process. Lett.*, vol. 15, pp. 5–8, Jan. 2008.

[20] B. Widrow, J. M. McCool, M. G. Larimore, and C. R. Johnson, "Stationary and nonstationary learning characteristics of the LMS adaptive filter," *Proc. IEEE*, vol. 64, no. 8, pp. 1151–1162, Aug. 1976.

[21] C. Paleologu, J. Benesty, and S. Ciochina, "A robust variable forgetting factor recursive least-squares algorithm for system identification," *IEEE Signal Process. Lett.*, vol. 15, pp. 597–600, Oct. 2008.

[22] A. Anghel, R. Cacoveanu, A. Moldovan, B. Rommen, and M. Datcu, "COBIS: Opportunistic C-band bistatic SAR differential interferometry," *IEEE J. Sel. Topics Appl. Earth Observ. Remote Sens.*, vol. 12, no. 10, pp. 3980–3998, Oct. 2019.

[23] L. Sornmo, P. O. Borjesson, M. E. Nygards, and O. Pahlm, "A method for evaluation of QRS shape features using mathematical model for the ECG," *IEEE Trans. Biomed. Eng.*, vol. BME-28, no. 10, pp. 713–717, Oct. 1981.

[24] P. S. Hamilton and W. J. Tompkins, "Adaptive matched filtering for QRS detection," in *Proc. Annu. Int. Conf. IEEE Eng. Med. Biol. Soc.*, New Orleans, LA, USA, 1988, pp. 147–148.

[25] M. Masjedi, M. Modarres-Hashemi, and S. Sadri, "Direct path and multipath cancellation in passive radars using subband variable step-size LMS algorithm," in *Proc. 19th Iranian Conf. Elect. Eng.*, 2011, pp. 1–5.

[26] F. Colone, D. W. O'Hagan, P. Lombardo, and C. J. Baker, "A multistage processing algorithm for disturbance removal and target detection in passive bistatic radar," *IEEE Trans. Aerosp. Electron. Syst.*, vol. 45, no. 2, pp. 698–722, Apr. 2009.

[27] M. Tudose, A. Anghel, R. Cacoveanu, and M. Datcu, "Electronic target for bistatic/monostatic SAR systems," in *Proc. 12th Eur. Conf. Synthetic Aperture Radar*, Aachen, Germany, 2018, pp. 1–5.

[28] F. Rosu, A. Anghel, and S. Ciochina, "Sub-resolution multipath mitigation in radar transponders by range compression and adaptive filtering," in *Proc. Int. Symp. Signals Circuits Syst.*, 2019, pp. 1–4.

**Filip Rosu** received the M.Sc. degree in communication circuits and systems in 2018 from the University POLITEHNICA of Bucharest (UPB), Bucharest, Romania, where he is currently working toward the Ph.D. degree in multistatic SAR with the Research Center for Spatial Information (CEOSpaceTech).

His research at CEOSpaceTech is focused on multistatic synthetic aperture radar, mostly for Earth Observation applications. He is currently a Radar Signal Processing Engineer with NXP Semiconductors, Bucharest, Romania, where he has had 6 U.S. patent applications filed since 2020. At NXP Semiconductors, his research is focused on signal processing for the future generation of imaging radar systems used in assisted and autonomous driving. His interests include radar, signal processing, and RF system design.

Mr. Rosu was a recipient of Best Student Paper by the International Conference on Communications (COMM) committee in 2018.

**Andrei Anghel** (Senior Member, IEEE) received the Engineering degree (as valedictorian) and the M.S. degree (with the highest grade) in electronic engineering and telecommunications from the University POLITEHNICA of Bucharest, Bucharest, Romania, in 2010 and 2012, respectively, the joint Ph.D. degree in signal, image, speech, and telecoms from the University of Grenoble Alpes, Grenoble, France, and in electronic engineering and telecommunications from the University POLITEHNICA of Bucharest, in 2015 (awarded with the *summa cum laude* distinction), and the Habilitation degree in electronic engineering, telecommunications, and information technologies from the University POLITEHNICA of Bucharest, in 2020.

Between 2012 and 2015, he was a Doctoral Researcher with Grenoble Image Speech Signal Automatics Laboratory, Grenoble, France. In 2012, he joined the University POLITEHNICA of Bucharest as a Teaching Assistant, where he is currently an Associate Professor with the Telecommunications Department (Faculty of Electronics, Telecommunications and Information Technology) and a Researcher with the Research Centre for Spatial Information—CEOSpaceTech. He is the author of more than 50 scientific publications, two textbooks, and a book about SAR signal processing for infrastructure monitoring. His current research interests include remote sensing, radar, microwaves, and signal processing.

Dr. Anghel regularly acts as a Reviewer for several IEEE and IET journals. He was a recipient of the "Traian Vuia" Prize by the Romanian Academy in 2021 for his work on bistatic radar systems with a fixed ground-based receiver and spaceborne transmitter of opportunity. He was also the recipient of two gold medals at the International Physics Olympiads in 2005 and 2006.
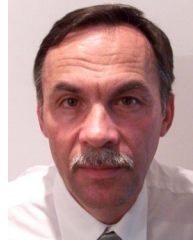
**Silviu Ciochină** (Life Senior Member, IEEE) received the master's degree in electronics and telecommunications and the Ph.D. degree in communications from the University POLITEHNICA of Bucharest (UPB), Bucharest, Romania, in 1971 and 1978, respectively.

He is currently a Professor with the UPB and was the Head of the Telecommunications Department (between 2004 and 2016). He has been involved in many national and international R&D projects in the areas of communications, signal processing, and radar. He was the Coordinator of the Romanian teams implied in the FP6 projects ATHENA (STREP–507312), ENTHRONE 1 (IP–507637), and ENTHRONE 2 (IP–038463). He has authored about 200 papers published in international journals and conference proceedings, seven of them being distinguished with "paper award." He has authored or coauthored more than ten books, three of them were published by international book publishers. His main areas of interest include digital signal processing, adaptive algorithms, and wireless communication technologies.

Prof. Ciochină has served as reviewer for many IEEE, Elsevier, Willey journals. He was awarded by Romanian Academy (Traian Vuia Award in 1981 and Gheorghe Cartianu Award in 1999), Education Ministry, and Defense Ministry (for works in the radar field).

**Remus Cacoveanu** received the M.S. degree in electronics and telecommunications from the University POLITEHNICA of Bucharest (UPB), Bucharest, Romania, in 1983, and the Ph.D. degree in microwave, optics, and optoelectronics from the Institut National Polytechnique de Grenoble, Grenoble, France, in 1997.

He is currently an Associate Professor in telecommunications with UPB. For more than ten years, he was the Technical Lead of the Redline Communications' Romanian branch, and between 2011 and 2015, he was Technical Consultant for Blinq Networks Canada. Since 2016, he has been a Lead Scientist with EOS Electronic Systems, Bucharest, Romania. His main fields of expertise are in the wireless communication systems, antennas, radar sensors, propagation, and microwave circuits.

**Mihai Datcu** (Fellow, IEEE) received the M.S. and Ph.D. degrees in electronics and telecommunications from the University POLITEHNICA of Bucharest (UPB), Bucharest, Romania, in 1978 and 1986, respectively, and the Habilitation a Diriger Des Recherches degree in computer science from the University Louis Pasteur, Strasbourg, France, in 1999.

Since 1981, he has been a Professor with the Department of Applied Electronics and Information Engineering, Faculty of Electronics, Telecommunications and Information Technology, UPB. Since 1993, he has been a Scientist with the German Aerospace Center, Weßling, Germany. He has held a Visiting Professor appointments with the University of Oviedo, Oviedo, Spain, the University Louis Pasteur, Strasbourg, France, the International Space University, Strasbourg, France, University of Siegen, Siegen, Germany, University of Innsbruck, Innsbruck, Austria, University of Alcala, Alcala, Spain, University Tor Vergata, Rome, Italy, University of Trento, Trento, Italy, Unicamp, Campinas, Brazil, China Academy of Science, Shenyang, China, Universidad Pontificia de Salamanca, campus de Madrid, Spain, University of Camerino, Camerino, Italy, and the Swiss Center for Scientific Computing, Manno, Switzerland. From 1992 to 2002, he had an Invited Professor Assignment with the Swiss Federal Institute of Technology (ETH Zurich), Zurich, Switzerland. Since 2001, he has been initiating and leading the Competence Center on Information Extraction and Image Understanding for Earth Observation, Paris Institute of Technology (ParisTech), Paris, France, a collaboration of DLR with the French Space Agency (CNES). He has been a Professor holder of the DLRCNES Chair with ParisTech. He has initiated the European frame of projects for image information mining and is involved in research programs for information extraction, data mining and knowledge discovery, and data science with the ESA, NASA, and in a variety of national and European projects. He is the Director of the Research Center for Spatial Information, UPB. He is a Senior Scientist and the Data Intelligence and Knowledge Discovery Research Group Leader with the Remote Sensing Technology Institute, DLR and delegate in the DLR-ONERA Joint Virtual Center for AI in Aerospace. He is a member of the ESA Working Group Big Data from Space and Visiting Professor withe ESA's-Lab. His research interests include explainable and physics aware artificial intelligence, smart radar sensors design, and quantum machine learning with applications in earth observation.

Dr. Datcu was a recipient of the National Order of Merit with the rank of Knight, for outstanding international research results, awarded by the President of Romania, in 2008, the Romanian Academy Prize Traian Vuia for the development of the system for automated analysis of digital images analysis system and his activity in image processing in 1987, and the Chaire d'excellence internationale Blaise Pascal 2017 for international recognition in the field of data science in earth observation. He has served as a Coorganizer for international conferences and workshops and as a Guest Editor for a special issues on AI and Big Data of the IEEE and other journals. He is the Representative of Romanian in the Earth Observation Program Board.